

# PAMELA - A Payload for Antimatter Matter Exploration and Light-nuclei Astrophysics

P. Picozza<sup>a</sup>, A.M. Galper<sup>b</sup>, G. Castellini<sup>d</sup>, O. Adriani<sup>c</sup>,  
 F. Altamura<sup>a</sup>, M. Ambriola<sup>j</sup>, G.C. Barbarino<sup>g</sup>, A. Basili<sup>a</sup>,  
 G.A. Bazilevskaia<sup>l</sup>, R. Bencardino<sup>a</sup>, M. Boezio<sup>e</sup>,  
 E.A. Bogomolov<sup>k</sup>, L. Bonechi<sup>c</sup>, M. Bongi<sup>c</sup>, L. Bongiorno<sup>i</sup>,  
 V. Bonvicini<sup>e</sup>, F. Cafagna<sup>j</sup>, D. Campana<sup>g</sup>, P. Carlson<sup>f</sup>,  
 M. Casolino<sup>a</sup>, C. De Marzo<sup>j,\*</sup>, M.P. De Pascale<sup>a</sup>, G. De Rosa<sup>g</sup>,  
 D. Fedele<sup>c</sup>, P. Hofverberg<sup>f</sup>, S.V. Koldashov<sup>b</sup>, S.Yu. Krutkov<sup>k</sup>,  
 A.N. Kvashnin<sup>l</sup>, J. Lund<sup>f</sup>, J. Lundquist<sup>e</sup>, O. Maksumov<sup>l</sup>,  
 V. Malvezzi<sup>a</sup>, L. Marcelli<sup>a</sup>, W. Menn<sup>h</sup>, V.V. Mikhailov<sup>b</sup>,  
 M. Minori<sup>a</sup>, S. Misin<sup>l</sup>, E. Mocchiutti<sup>e</sup>, A. Morselli<sup>a</sup>,  
 N.N. Nikonov<sup>k</sup>, S. Orsi<sup>f</sup>, G. Osteria<sup>g</sup>, P. Papini<sup>c</sup>,  
 M. Pearce<sup>f,\*\*</sup>, M. Ricci<sup>i</sup>, S.B. Ricciarini<sup>c</sup>, M.F. Runtso<sup>b</sup>,  
 S. Russo<sup>g</sup>, M. Simon<sup>h</sup>, R. Sparvoli<sup>a,\*\*\*</sup>, P. Spillantini<sup>c</sup>,  
 Yu.I. Stozhkov<sup>l</sup>, E. Taddei<sup>c</sup>, A. Vacchi<sup>e</sup>, E. Vannuccini<sup>c</sup>,  
 S.A. Voronov<sup>b</sup>, Y.T. Yurkin<sup>b</sup>, G. Zampa<sup>e</sup>, N. Zampa<sup>e</sup>,  
 V.G. Zverev<sup>b</sup>

<sup>a</sup>*INFN, Structure of Rome "Tor Vergata" and Physics Department of University of Rome "Tor Vergata", Via della Ricerca Scientifica 1, I-00133 Rome, Italy*

<sup>b</sup>*Moscow Engineering and Physics Institute, Kashirskoe Shosse 31, RU-115409 Moscow, Russia*

<sup>c</sup>*INFN, Structure of Florence and Physics Department of University of Florence, Via Sansone 1, I-50019 Sesto Fiorentino, Florence, Italy*

<sup>d</sup>*IFAC, Via Madonna del Piano 10, I-50019 Sesto Fiorentino, Florence, Italy*

<sup>e</sup>*INFN, Structure of Trieste and Physics Department of University of Trieste, Via A. Valerio 2, I-34127 Trieste, Italy*

<sup>f</sup>*KTH, Department of Physics, Albanova University Centre, SE-10691 Stockholm, Sweden*

<sup>g</sup>*INFN, Structure of Naples and Physics Department of University of Naples "Federico II", Via Cintia, I-80126 Naples, Italy*

<sup>h</sup>*Universität Siegen, D-57068 Siegen, Germany*

<sup>i</sup>*INFN, Laboratori Nazionali di Frascati, Via Enrico Fermi 40, I-00044 Frascati, Italy*

<sup>j</sup>*INFN, Structure of Bari and Physics Department of University of Bari, Via  
Amendola 173, I-70126 Bari, Italy*

<sup>k</sup>*Ioffe Physical Technical Institute, Polytekhnicheskaya 26, RU-194021 St.  
Petersburg, Russia*

<sup>ℓ</sup>*Lebedev Physical Institute, Leninsky Prospekt 53, RU-119991 Moscow, Russia*

---

## Abstract

The PAMELA experiment is a satellite-borne apparatus designed to study charged particles in the cosmic radiation with a particular focus on antiparticles. PAMELA is mounted on the Resurs DK1 satellite that was launched from the Baikonur cosmodrome on June 15<sup>th</sup> 2006. The PAMELA apparatus comprises a time-of-flight system, a magnetic spectrometer, a silicon-tungsten electromagnetic calorimeter, an anticoincidence system, a shower tail catcher scintillator and a neutron detector. The combination of these devices allows antiparticles to be reliably identified from a large background of other charged particles. This paper reviews the design, space qualification and on-ground performance of PAMELA. The in-orbit performance will be discussed in future publications.

---

## 1 Introduction

The PAMELA (a Payload for Antimatter Matter Exploration and Light-nuclei Astrophysics) experiment is a satellite-borne apparatus designed to study charged particles in the cosmic radiation with a particular focus on antiparticles (antiprotons and positrons). PAMELA is installed inside a pressurized container attached to a Russian Resurs DK1 earth-observation satellite that was launched into space by a Soyuz-U rocket on June 15<sup>th</sup> 2006 from the Baikonur cosmodrome in Kazakhstan. The satellite orbit is elliptical and semi-polar, with an altitude varying between 350 km and 600 km, at an inclination of 70°. The mission is foreseen to last for at least three years.

The PAMELA mission is devoted to the investigation of dark matter, the baryon asymmetry in the Universe, cosmic ray generation and propagation in our galaxy and the solar system, and studies of solar modulation and the interaction of cosmic rays with the Earth's magnetosphere. The primary scientific goal is the study of the antimatter component of the cosmic radiation,

---

\* Deceased.

\*\*Corresponding author. e-mail: pearce@particle.kth.se

\* \*Corresponding author. e-mail: roberta.sparvoli@roma2.infn.it

Table 1

Design goals for PAMELA performance.

<b>Cosmic-ray particle</b>	<b>Energy range</b>
Antiprotons	80 MeV - 190 GeV
Positrons	50 MeV - 270 GeV
Electrons	50 MeV - 400 GeV
Protons	80 MeV - 700 GeV
Electrons+positrons	up to 2 TeV
Light nuclei (up to Z=6)	100 MeV/n - 700 GeV/n
Antinuclei	of the order of $10^{-7}$

- in order to search for evidence of dark matter particle (e.g. non-hadronic particles outside the Standard Model) annihilations by precisely measuring the antiparticle (antiproton and positron) energy spectra;
- in order to search for antinuclei (in particular, anti-helium);
- in order to test cosmic-ray propagation models through precise measurements of the antiparticle energy spectrum and precision studies of light nuclei and their isotopes.

Concomitant goals include,

- a study of solar physics and solar modulation during the 24<sup>th</sup> solar minimum by investigating low energy particles in the cosmic radiation;
- reconstructing the cosmic ray electron energy spectrum up to several TeV thereby allowing a possible contribution from local sources to be studied.

Table 1 shows the design goals for PAMELA performance. The various cosmic-ray components and energy ranges over which PAMELA will provide new results are presented.

Antiparticle measurements are the main scientific goal of the experiment. The precise determination of the antiproton and positron energy spectra will provide important information concerning cosmic-ray propagation and solar modulation. For example, indications of charge dependent solar modulation effects have been already seen in the antiproton to proton ratio data [1]. Antiparticles could also be produced from exotic sources such as primordial black holes [2] or the annihilation of supersymmetric [3] or Kaluza-Klein [4,5] dark matter particles. Figures 1 and 2 show the current status of cosmic-ray antiproton and positron energy spectrum measurements, respectively. Theoretical calculations for pure secondary production [6,7,8,9] and for pure primary production due to the annihilation of supersymmetric dark matter particles [10,11] are also shown. Almost all data available so far have been obtained by balloon-borne

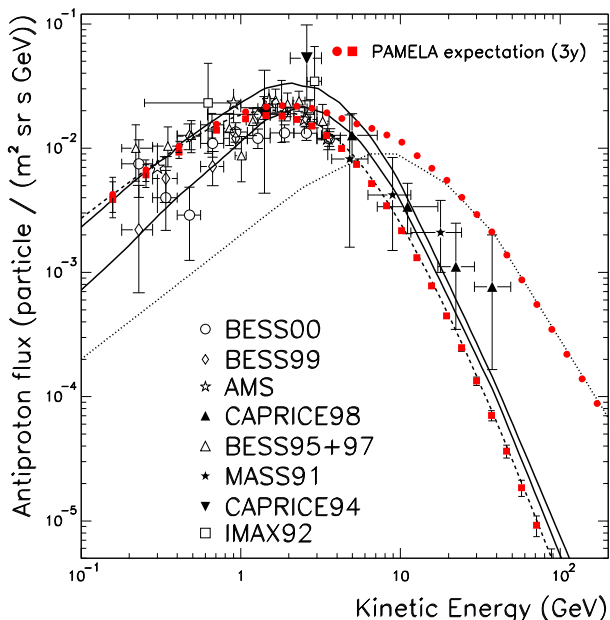


Fig. 1. Recent experimental  $\bar{p}$  spectra (BESS00 and BESS99 [1], AMS [17], CAPRICE98 [18], BESS95+97 [19], MASS91 [20], CAPRICE94 [21], IMAX92 [22]) along with theoretical calculations for pure  $\bar{p}$  secondary production (solid lines: [6], dashed line: [7]) and for pure  $\bar{p}$  primary production (dotted line: [10], assuming the annihilation of neutralinos of mass  $964 \text{ GeV}/c^2$ ). The expected PAMELA performance, in case of a pure secondary component (full boxes) and of an additional primary component (full circles), are indicated. Only statistical errors are included in the expected PAMELA data.

experiments. PAMELA will be able to perform very precise measurements with high statistics ( $\sim 10^4 \bar{p}$  and  $\sim 10^5 e^+$  per year) and over a wider energy range than possible to date. The full boxes in figures 1 and 2 indicate the expected PAMELA performance in case of a pure secondary antiproton and positron components and the full circles show the expected performance in case of an additional primary component. The errors on the expected PAMELA data points only include statistical uncertainties. An average PAMELA orbit has been used to estimate the vertical geomagnetic cut-offs and, consequently, the expected number of antiproton and positron events at low energies [14].

Another prominent goal of PAMELA is to measure the antihelium/helium ratio with a sensitivity of the order of  $10^{-7}$ . This would represent a factor of 50 improvement on contemporary limits, as shown in figure 3 as a function of rigidity (momentum /charge) [12]. The contribution to the antihelium flux from cosmic ray interactions is expected to be less than  $10^{-12}$  [13] and so an observation of antihelium would be a significant discovery as it could indicate the presence of antimatter domains in a baryon symmetric Universe.

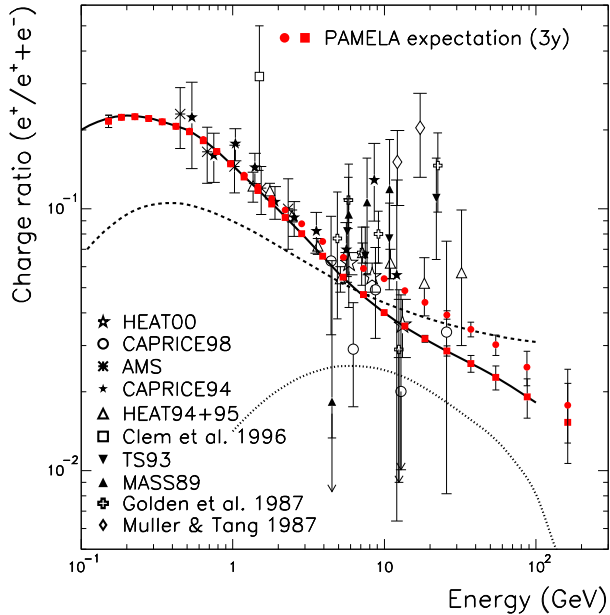


Fig. 2. The positron fraction as a function of energy measured by several experiments ([23,24,25] and MASS89 [26], TS93 [27], HEAT94+95 [28], CAPRICE94 [29], AMS [30], CAPRICE98 [31], HEAT00 [32]). The dashed [8] and the solid [9] lines are calculations of the secondary positron fraction. The dotted line is a possible contribution from annihilation of neutralinos of mass  $336 \text{ GeV}/c^2$  [11]. The expected PAMELA performance, for a pure secondary component (full boxes) and of an additional primary component (full circles), are indicated. Only statistical errors are included in the expected PAMELA data.

The quasi-polar orbit and low geomagnetic cut-off experienced by the PAMELA apparatus combined with its intrinsic ability to measure low momenta will allow phenomena connected with solar and earth physics to be investigated [15].

The ability to measure the combined electron and positron energy spectrum up to 2 TeV will allow the contribution of local sources to the cosmic radiation to be investigated (e.g. see [16]).

This article is organized as follows. The subdetector components of the PAMELA instrument are discussed in section 2 along with results from performance studies with particle beams and cosmic rays. The data acquisition and trigger systems are described in section 3. The Resurs DK1 satellite which houses PAMELA is presented in section 4. Tests on various qualification models of the PAMELA apparatus are summarised in section 5. The physics performance of the flight instrument is presented in section 6.

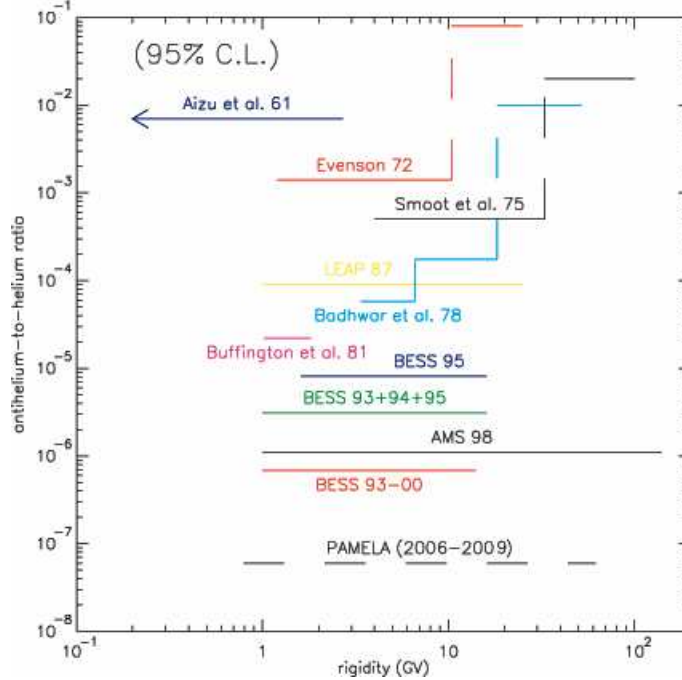


Fig. 3. The ratio of anti-helium to helium in the cosmic radiation shown as a function of rigidity [12]. No observation of antihelium has been made to date and so upper limits are shown. The expectation for PAMELA after a 3 year long mission is shown.

## 2 The PAMELA apparatus

The PAMELA apparatus is composed of the following subdetectors, arranged as shown in figure 4:

- a time of flight system (ToF: S1, S2, S3);
- a magnetic spectrometer;
- an anticoincidence system (CARD, CAT, CAS);
- an electromagnetic calorimeter;
- a shower tail catcher scintillator (S4);
- a neutron detector.

The apparatus is  $\sim 1.3$  m high, has a mass of 470 kg and an average power consumption of 355 W. The masses are distributed according to table 2 and the power consumption according to table 3.

### 2.1 Overview

PAMELA is built around a 0.43 T permanent magnet spectrometer equipped with 6 planes of double-sided silicon detectors allowing the sign, absolute value of charge and momentum of traversing charged particles to be determined. The

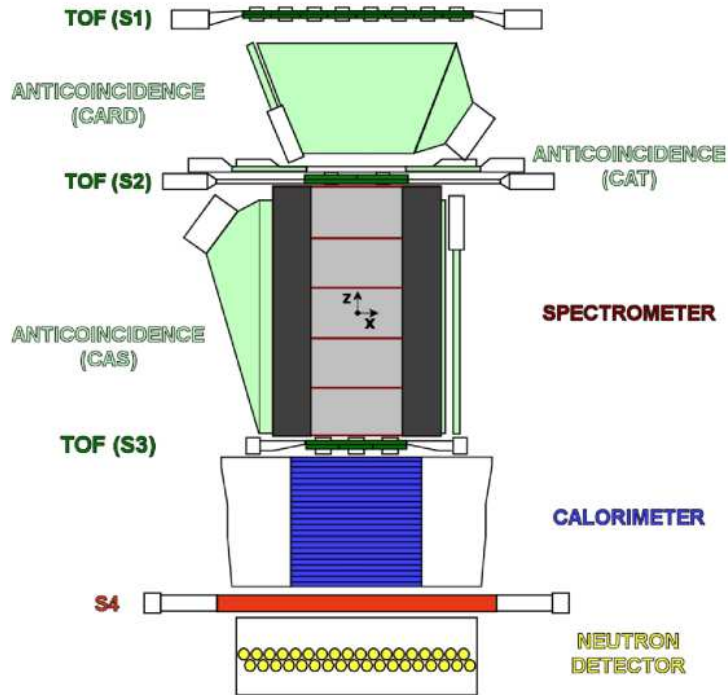


Fig. 4. The PAMELA instrument. Top: a schematic overview of the apparatus. Bottom: a photograph taken just prior delivery to Russia for integration with the Resurs DK1 satellite. The detector is approximately 1.3 m tall. The magnetic field lines in the spectrometer are oriented along the  $y$  direction.

Table 2

The PAMELA mass budget.

<b>Subsystem</b>	<b>Mass (kg)</b>
Spectrometer	127
Calorimeter	104
General mechanics	85
Electronic units	45
Neutron Detector	30
Thermal system	22
Time-Of-Flight	18
Anticoincidence	16
Magnetic screens	15
Bottom Scintillator	8
<b>Total Mass</b>	<b>470</b>

Table 3

The PAMELA average power budget.

<b>Subsystem</b>	<b>Power (W)</b>
Electronics	80
DC/DC converters	74
Spectrometer	63
Calorimeter	55
CPU	35
Power Supply system	35
Neutron Detector	10
Anticoincidence	1
Bottom Scintillator	1
Time-Of-Flight	1
<b>Total Power</b>	<b>355</b>

acceptance of the spectrometer (which also defines the overall acceptance of the PAMELA experiment) is  $21.5 \text{ cm}^2\text{sr}$  and the maximum detectable rigidity is  $\sim 1 \text{ TV}$ . Spillover effects limit the upper detectable antiparticle momentum to  $\sim 190 \text{ GeV}/c$  ( $\sim 270 \text{ GeV}/c$ ) for antiprotons (positrons). The spectrometer is surrounded by a plastic scintillator veto shield. An electromagnetic calorimeter mounted below the spectrometer measures the energy of incident electrons and



allows topological discrimination between electromagnetic and hadronic showers (or non-interacting particles). Planes of plastic scintillator mounted above and below the spectrometer form a time-of-flight system which also provides the primary experimental trigger. The timing resolution of the time-of-flight system allows albedo particles to be identified and proton-electron separation is also possible below  $\sim 1$  GeV/c. Ionising energy loss measurements in the time-of-flight scintillator planes and the silicon planes of the magnetic spectrometer allow the absolute charge of traversing particles to be determined. The volume between the upper two time-of-flight planes is bounded by an additional plastic scintillator anticoincidence system. A plastic scintillator system mounted beneath the calorimeter provides an additional stand-alone trigger for high energy electrons and is followed by a neutron detection system for the selection of very high energy electrons (up to 2 TeV) which shower in the calorimeter but do not necessarily pass through the spectrometer.

The PAMELA subdetectors are read out and controlled by a data acquisition system based around Actel (54SX series) Field Programmable Gate Arrays (FPGA) [33] and Analog Devices (ADSP-2187L) Digital Signal Processors (DSP) [34]. Connections between different systems are realised with redundant data-strobe [35] Low Voltage Differential Signaling (LVDS) links. Each subdetector is also connected to a global trigger system and can issue alarm conditions (e.g. over-temperature, data corruption) to a housekeeping system. All the data acquisition boards (except for the calorimeter) are housed in a custom crate secured to the PAMELA superstructure, as shown in figure 4 (bottom). In order to promote reliability, common design rules have been followed for all electronics systems in PAMELA, e.g. over-current protection on all electronics boards, redundant data links, redundant power connections and the use of radiation qualified components.

## 2.2 *The Time of Flight (ToF) system*

The ToF system [36] comprises 6 layers of fast plastic scintillators (Bicron BC-404 [37]) arranged in three planes (S1, S2 and S3), with alternate layers placed orthogonal to each other, as shown in figure 5. The distance between S1 and S3 is 77.3 cm. Time-of-flight information for charged particles passing between planes S1 and S3 is combined with track length information derived from the magnetic spectrometer (see section 2.4) to determine particle velocities and reject albedo particles. Ionisation (dE/dx) measurements in the scintillator layers allow the particle charge to be determined at least up to  $Z=8$ . Coincidental energy deposits in combinations of planes provide the main trigger for the experiment, as described in section 3.2. The segmentation of each plane allows redundant studies of the trigger efficiency.

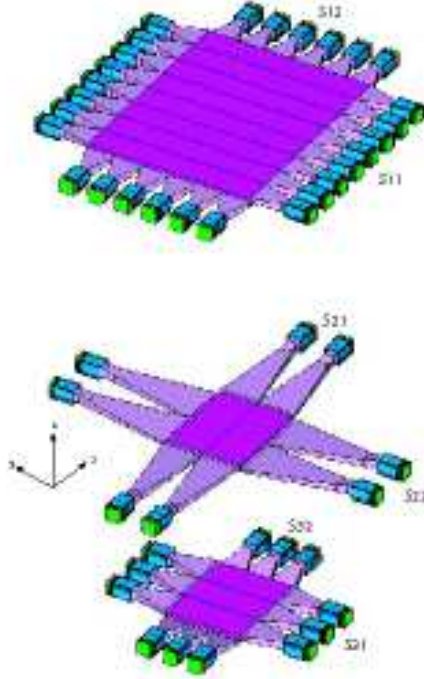


Fig. 5. A schematic overview of the Time of Flight system. The distance between the S1 and S3 planes is 77.3 cm.

The sensitive area of each of the two S1 layers is  $(33 \times 40.8)$  cm<sup>2</sup> with the first layer divided into 8 bars and the second layer divided into 6 bars. The total sensitive area of the S2 and S3 planes is  $(15 \times 18)$  cm<sup>2</sup> segmented into  $2 \times 2$  and  $3 \times 3$  orthogonal bars, respectively. The S1 and S3 layers are 7 mm thick while the S2 layers are 5 mm thick. There are 24 scintillator bars in total. Both ends of each scintillator bar are glued to a plastic light guide which is mechanically coupled to a Hamamatsu R5900U photomultiplier (PMT) by means of silicone pads of thickness 3 mm and 6 mm. The scintillators and light-guides are wrapped in 2 layers of 25  $\mu$ m thick Mylar foil. The S3 plane is mounted directly on the base plate of PAMELA, while the other two planes are enclosed in light-proof boxes suspended off the PAMELA structure. A high-voltage divider circuit is mounted directly behind each PMT. The high-voltage and discrimination threshold for each PMT is chosen to optimize the performance of a given ToF bar.

The ToF electronics system converts the 48 PMT pulses into time- and charge-based measurements. In the timing section, a capacitor is linearly charged during a time interval defined by the passage of a particle through the ToF system. In the charge section, a capacitor is charged with the PMT pulse charge. In both cases, during read out the capacitor is linearly discharged into a time-to-digital converter. The ToF electronics system comprises a nine board electronics system based around the PAMELA-standard FPGAs and DSPs. A separate trigger board processes signals [38] from the 48 PMTs as well as trigger signals from the calorimeter and bottom scintillator (see section 3.2).

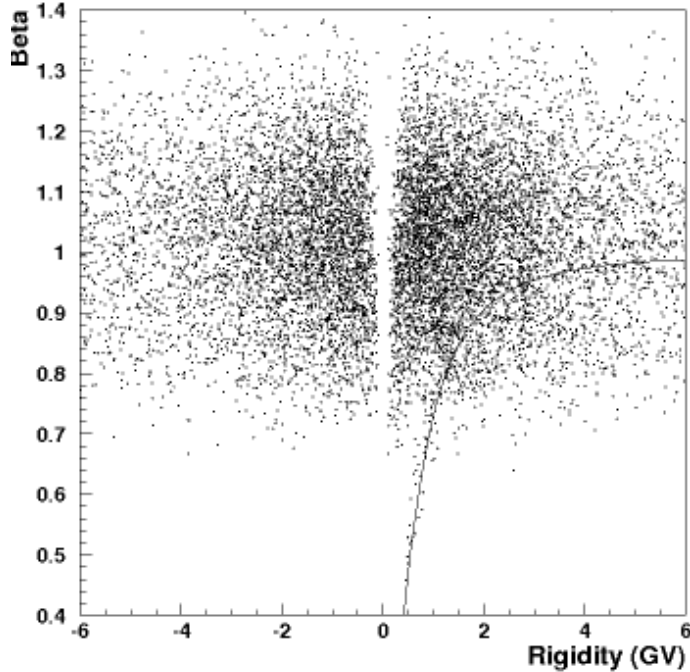


Fig. 6. The particle velocity measured by the ToF system as a function of rigidity. The solid line is the theoretical  $\beta$  for protons. The figure comprises 46000 events acquired with the final ToF system at ground.

Rate counters, dead-/live-time counters and the logic to generate calibration pulse sequences for different subsystems are also implemented. Control masks select trigger types (see section 3.2) and allow noisy or dead PMT channels to be vetoed and the PMT hit pattern to be recorded for each trigger.

Figure 6 shows the velocity of particles (in units of speed of light,  $\beta$ ) measured by the ToF system as a function of their rigidity for data recorded at ground. Most of the events are relativistic muons. A small proton component is visible at low rigidity (the solid line indicates the theoretical  $\beta$  for protons). The measured time-of-flight resolution of  $\sim 250$  ps will allow electrons (positrons) to be separated from antiprotons (protons) up to  $\sim 1$  GeV/c. Albedo particles can also be rejected with a significance of 60 standard deviations. In addition, the measurement of ionization losses in the ToF scintillators will allow the determination of the absolute charge of the particles, as shown in figure 7. These data were collected during a beam test performed at the GSI facility in Darmstadt. Prototype versions of the S1, S2 and S3 ToF paddles were exposed to  $^{12}\text{C}$  beams. Targets of aluminum and polyethylene were used to generate a variety of fragmentation products. During this test, the S1 and S2 layers were used to clean the data sample, and the particle charge was subsequently measured using the S3 layer. Data taken during this test also allowed the timing resolution for carbon to be determined as 70 ps.

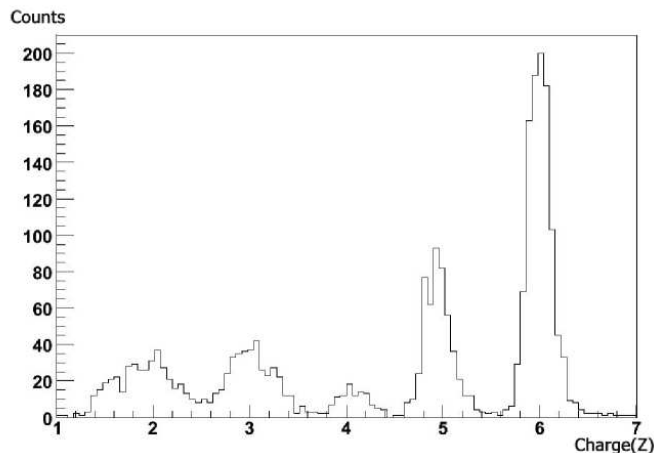


Fig. 7. Results from the GSI beam test. Energy deposits in prototype S3 scintillators are converted by an ADC to identify the secondaries produced by fragmentation of the initial 1200 MeV/c  $^{12}\text{C}$  beam.

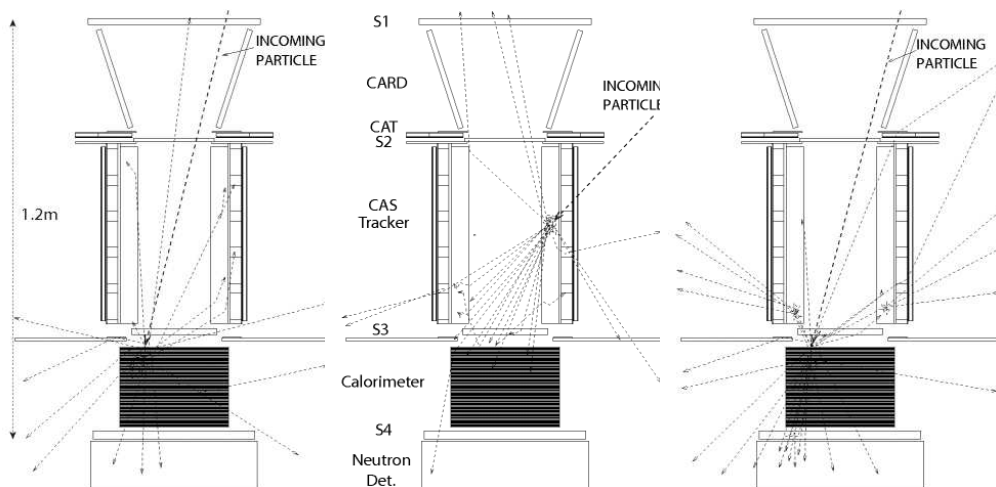


Fig. 8. Schematic representations of simulated proton interactions in the PAMELA apparatus. Left: a good trigger event without AC activity. Centre: a false trigger created by a particle entering the apparatus from the side generating a shower and AC activity. Right: Particles backscattered from the calorimeter can also give rise to AC activity for good trigger events.

### 2.3 Anticoincidence systems

Simulations have shown that the majority ( $\sim 75\%$ ) of triggers in orbit are “false” triggers [39], i.e. where the coincidental energy deposits in the time of flight scintillators are generated by secondary particles produced in the mechanical structure of the experiment, as shown in figure 8. The aim of the anticoincidence systems is to identify these events during offline data analysis, or through the use of a second-level trigger in-orbit (see section 3.2).

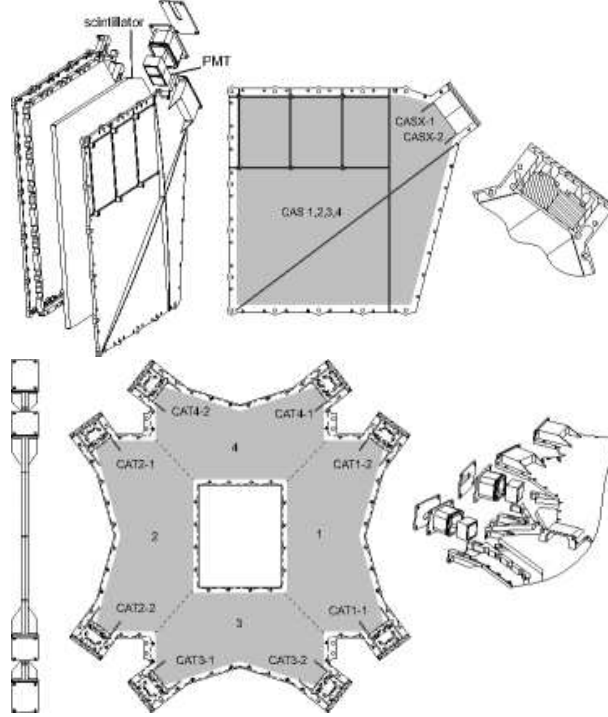


Fig. 9. An overview of the AC system. Top: the CAS system. Bottom: the CAT system. The CARD system is not shown but the design closely follows that of CAS. The CAS scintillator is approximately 40 cm tall and 33 cm wide. The hole in the CAT scintillator measures approximately 22 cm by 18 cm.

The PAMELA experiment contains two anticoincidence (AC) systems [40]. The primary AC system [41] consists of 4 plastic scintillators (CAS) surrounding the sides of the magnet and one covering the top (CAT), as shown in figure 9. A secondary AC system consists of 4 plastic scintillators (CARD) that surrounds the volume between the first two time-of-flight planes. The CARD detectors are scaled-down versions of CAS. The AC systems use 8 mm thick plastic scintillators (Bicron BC-448M [37]) read out by Hamamatsu R5900U PMTs. Each scintillator is covered in two layers of reflective Tyvek [42] material and coupled via a 7 mm thick silicone pad to the PMTs. Each CAS and CARD detector is read out by two identical PMTs in order to decrease the possibility of single point failure. Also for this reason, and to cover the irregularly shaped area, the CAT detector is read out by 8 PMTs. A high-voltage divider is mounted directly behind each PMT and operated at a fixed voltage of -800 V. The scintillators and PMTs are housed in aluminium containers which provide light-tightness, allow fixation to the PAMELA superstructure and ensure that a reliable scintillator-PMT coupling is maintained. The small fringe field from the magnetic spectrometer at the position of the PMTs means that additional magnetic shielding is not required.

The signals from the 24 PMTs are divided between two independent data acquisition boards with signals from PMTs for a given CAS or CARD detector

or CAT quadrant routed to different boards. Only binary hit information is stored from each PMT indicating whether the deposited energy exceeds 0.5 mip (where 1 mip is the most probable energy deposited by a minimum ionising particle). On each board, an analogue front-end electronics system comprising an integration/amplification and discrimination stage processes the PMT signals before they are fed into a FPGA. The core of this digital system is a 16 bit shift register allowing hit information to be recorded in a time window of length  $1.28 \mu\text{s}$  centered on the trigger time. Within this window the hit can be located with an accuracy of 80 ns. The FPGA also allows the PMT singles rates to be monitored and controls the data acquisition system. A DSP controls a monitoring system which is based around 640 nm miniature LEDs glued directly to the scintillator material.

The efficiency of the large area CAS detectors has been studied using an external drift chamber to map the spatial distribution of incident cosmic ray muons. A detection efficiency for mips of  $(99.91 \pm 0.04)\%$  was observed [43]. The AC system has also been tested by studying the backscattering of particles (see figure 8) from the calorimeter during tests with high energy particle beams [44]. The robustness of the AC system has been determined by studying the stability of the scintillator-PMT coupling to variations in temperature [43] and the vibration spectra expected during launch [45].

#### 2.4 *Magnetic spectrometer*

The central part of the PAMELA apparatus is a magnetic spectrometer [46] consisting of a permanent magnet and a silicon tracker. The magnetic spectrometer is used to determine the sign of charge and the rigidity of particles up to  $\sim 1 \text{ TV}/c$ . Ionisation loss measurements are also made in the silicon planes, allowing absolute particle charge to be determined up to at least  $Z=6$ .

The magnet is composed of five modules forming a tower 44.5 cm high. Each module comprises twelve magnetic blocks, made of a Nd-Fe-B alloy with a residual magnetisation of 1.3 T. The blocks are configured to provide an almost uniform magnetic field oriented along the y-direction inside a cavity of dimensions  $(13.1 \times 16.1) \text{ cm}^2$ . The dimensions of the permanent magnet define the geometrical factor of the PAMELA experiment to be  $21.5 \text{ cm}^2\text{sr}$ . To allow precise rigidity measurements to be obtained from the reconstructed particle trajectory, the magnetic field has been precisely measured with a Hall probe through-out the cavity volume and the surrounding regions. Figure 10 shows the y-component of the magnetic field measured in the  $z=0$  plane as a function of x and y and the y-component as measured along the z-axis. The mean magnetic field inside the cavity is 0.43 T with a value of 0.48 T measured at the centre. Any stray magnetic field outside of the cavity can potentially

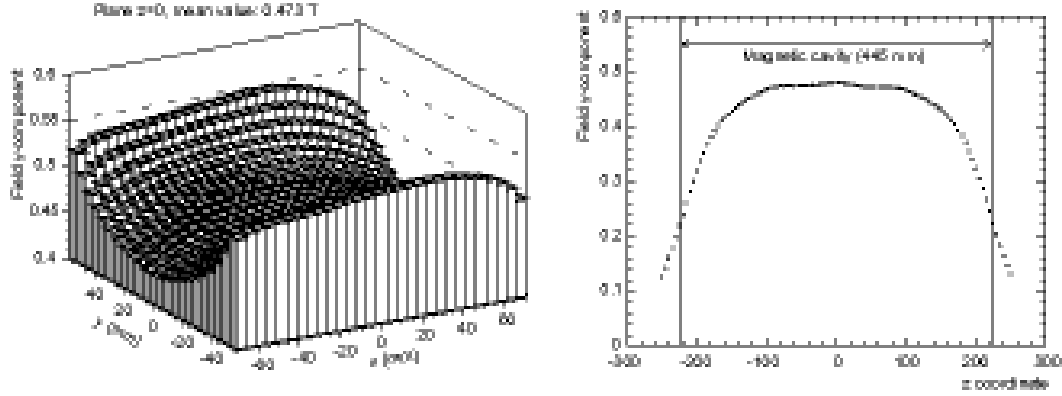


Fig. 10. Left: the y-component of the spectrometer magnetic field (T) measured at  $z=0$ . Right: the variation of the y-component of the spectrometer magnetic field (T) evaluated along the z-axis (mm).

interfere with the satellite instruments and navigation systems. In order to attenuate the stray field, the magnet is enclosed by ferromagnetic shielding.

Six equidistant  $300 \mu\text{m}$  thick silicon detector planes are inserted inside the magnetic cavity. The double-sided silicon sensors provide two independent impact coordinates on each plane. The basic detecting unit is the ladder which comprises two sensors,  $(5.33 \times 7.00) \text{ cm}^2$ , assembled with a front-end hybrid circuit, as shown in figure 11. Each plane is built from three ladders that are inserted inside an aluminum frame which connects to the magnet canister. In order to limit multiple scattering in dead layers, no additional supporting structure is present above or below the planes. Each high resistivity n-type silicon detector is segmented into micro-strips on both sides with  $p^+$  strips implanted on the junction side (bending-, x-view) and  $n^+$  strips on the Ohmic side (non-bending, y-view). In the x-view, the implantation pitch is  $25 \mu\text{m}$  and the read-out pitch is  $50 \mu\text{m}$ . In the y-view, the read-out pitch is  $67 \mu\text{m}$  with the strips orthogonal to those in the x-view. The mip efficiency for a single plane (including dead regions) exceeds 90%.

The front-end electronics system is based around VA1 Application Specific Integrated Circuits (ASICs) [47] which contain 128 charge sensitive preamplifiers connected to shapers and a sample and hold circuit. The signals from the VA1 chips are sent over 5 cm long kapton cables to be digitised by Analog-to-Digital (ADC) boards mounted on the magnet canisters. The digitised data are transferred by serial links to DSP-based read-out boards where they are compressed using a Zero Order Predictor (ZOP) algorithm. The compression factor is estimated at 95%.

The main task of the spectrometer is to measure the rigidity,  $R$ , of charged particles. The momentum of the particle and the sign of its electric charge can then be derived from the relation  $R = cp/Ze$ , where  $e$  is the electron charge,

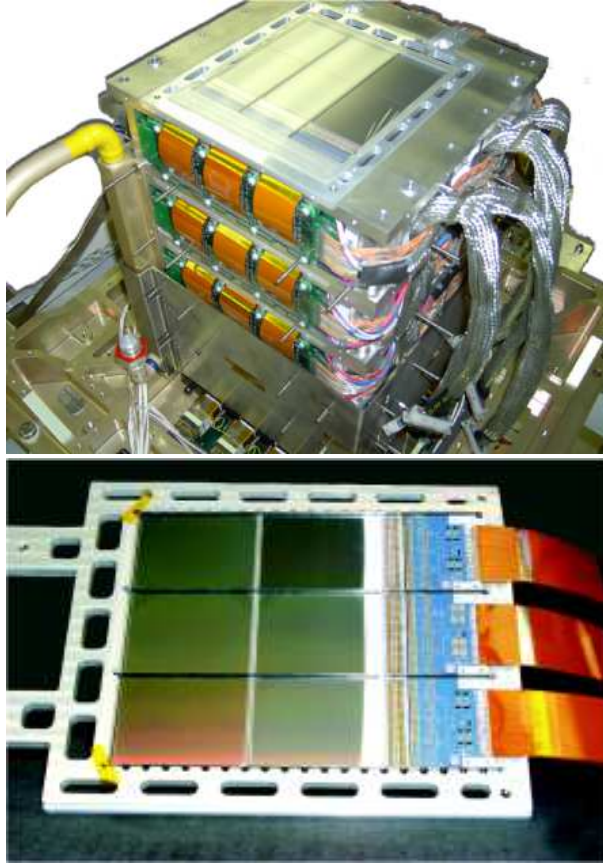


Fig. 11. Top: an overview of the magnetic spectrometer showing the top silicon plane. The magnet cavity has dimensions  $(13.1 \times 16.1) \text{ cm}^2$ . A cooling loop enters from the left-hand side and the ADC boards mounted on the magnet canister are also visible. The lower part of the magnet canister is covered by a magnetic screen. Bottom: a silicon plane comprising three silicon strip detectors and front-end electronics.

$p$  the momentum,  $c$  the speed of light and  $Z$  is the absolute charge.

The magnetic spectrometer measures the deflection of a particle, which is defined as the inverse of the rigidity. The resolution in the deflection measurement depends on the geometrical configuration of the spectrometer, on the intensity of the magnetic field and on the spatial resolution of the position measuring system - the silicon sensors in this case. This spatial resolution depends on the particle incidence angle. For normally incident tracks, tests with particle beams show a spatial resolution of  $(3.0 \pm 0.1) \mu\text{m}$  and  $(11.5 \pm 0.6) \mu\text{m}$  in the bending and non-bending views, respectively. The spatial resolution in the bending view is shown in figure 12 (left). Figure 12 (right) shows the resulting deflection error as a function of rigidity obtained with proton beams. From this plot a maximum detectable rigidity (MDR)<sup>1</sup> of  $\sim 1 \text{ TV}$  can be inferred. Note that this exceeds the design goal presented in table 1. In flight, the deflection measurement of the tracking system will be cross-checked with

<sup>1</sup> Defined as a 100% uncertainty in the rigidity determination.



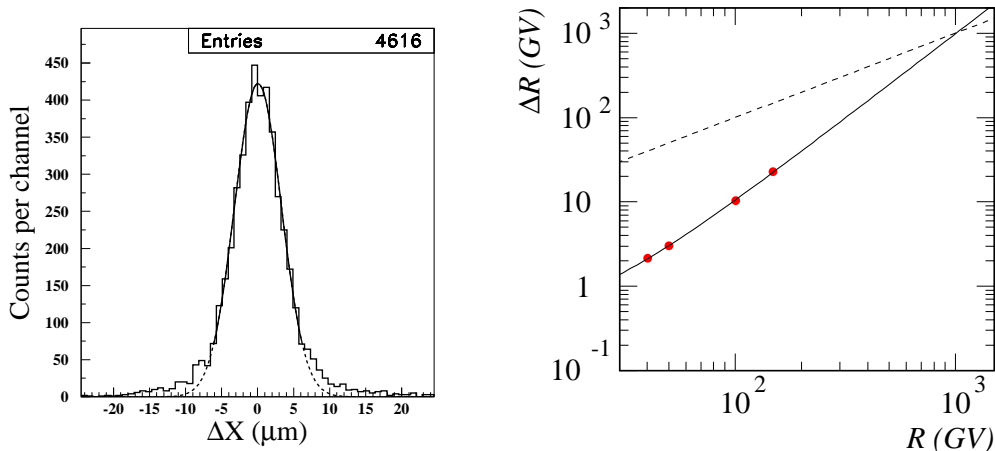


Fig. 12. Left: The spatial resolution of the tracker in the bending view. The line indicates a Gaussian fit. Right: the deflection error  $\Delta R$  measured by the magnetic spectrometer as a function of  $R$  obtained with proton beams. The dashed line is the bisector  $\Delta R = R$ ; the crossing point between this line and the experimental  $\Delta R$  curve gives the maximum detectable rigidity of the spectrometer.

the energy measurement of the calorimeter for high-energy electrons.

## 2.5 Electromagnetic Calorimeter

Protons and electrons dominate the positively and negatively charged components of the cosmic radiation, respectively. The main task of the calorimeter is to select positrons and antiprotons from like-charged backgrounds which are significantly more abundant. Positrons must be identified from a background of protons that increases from about  $10^3$  times the positron component at 1 GeV/c to  $\sim 5 \times 10^3$  at 10 GeV/c, and antiprotons from a background of electrons that decreases from  $\sim 5 \times 10^3$  times the antiproton component at 1 GeV/c to less than  $10^2$  times above 10 GeV/c. This means that the PAMELA system must separate electrons from hadrons at a level of  $10^5 - 10^6$ . Much of this separation must be provided by the calorimeter, i.e. electrons must be selected with an acceptable efficiency and with as small a hadron contamination as possible.

The sampling electromagnetic calorimeter comprises 44 single-sided silicon sensor planes (380  $\mu\text{m}$  thick) interleaved with 22 plates of tungsten absorber [53]. Each tungsten layer has a thickness of 0.26 cm, which corresponds to 0.74  $X_0$  (radiation lengths), giving a total depth of 16.3  $X_0$  ( $\sim 0.6$  nuclear interaction lengths). Each tungsten plate is sandwiched between two printed circuit boards upon which the silicon detectors, front-end electronics and ADCs are mounted. The (8 $\times$ 8)  $\text{cm}^2$  silicon detectors are segmented into 32 read-out strips with a



Fig. 13. Top: The PAMELA electromagnetic calorimeter with the topmost silicon plane visible. The device is  $\sim 20$  cm tall and the active silicon layer is  $\sim 24 \times 24$  cm<sup>2</sup> in cross-section. Bottom: Detail of a single calorimeter module comprising a tungsten layer sandwiched between two silicon detector planes.

pitch of 2.4 mm. The silicon detectors are arranged in a  $3 \times 3$  matrix and each of the 32 strips is bonded to the corresponding strip on the other two detectors in the same row (or column), thereby forming 24 cm long read-out strips. The orientation of the strips of two consecutive layers is orthogonal and therefore provides two-dimensional spatial information (“views”). Figure 13 shows the calorimeter prior to integration with the other PAMELA detectors.

The calorimeter front-end electronics is based around the CR1.4P ASIC [48] which provides 16 channels containing a charge-sensitive preamplifier, a CR-RC shaper, a track-and-hold circuit and an output multiplexer. A charge-injection calibration system is also implemented. Six CR1.4P chips are used per plane with the outputs multiplexed into a single 16-bit ADC. Data from all 44 ADCs are processed by 4 DSP-based read-out boards mounted within the calorimeter housing before being sent over serial links to the main PAMELA data acquisition system. The read-out is divided into 4 independent sections, corresponding to the x-even, y-even, x-odd and y-odd planes.

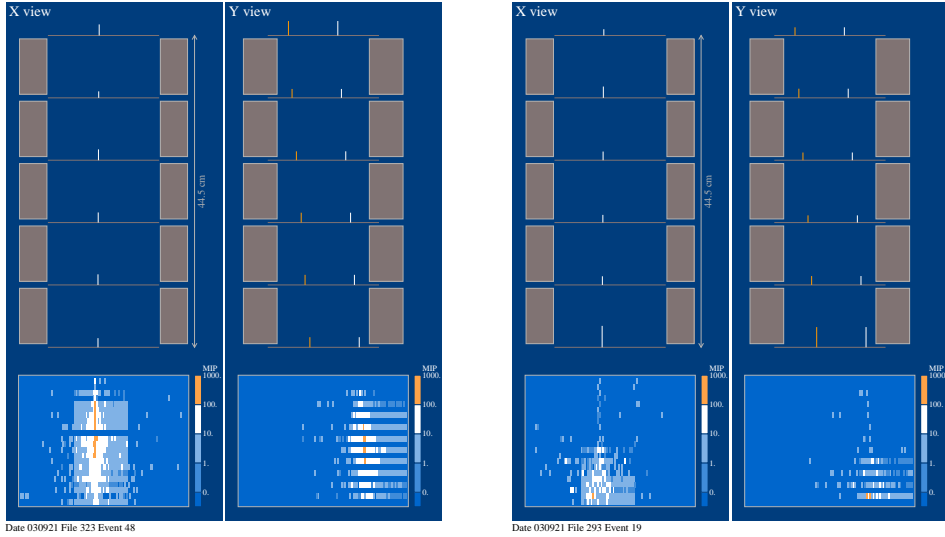


Fig. 14. An event display of a 50 GeV/c electron (left) and proton (right) recorded at the CERN SpS facility. Hits in the tracking system are shown (including ambiguities for the y-view) along with activity in the calorimeter. The signals from the odd planes of the y-view of the calorimeter were not read-out during this test. One of the x-view planes was also not operational and was later replaced.

The longitudinal and transverse segmentation of the calorimeter, combined with the measurement of the particle energy loss in each silicon strip, allows a high identification (or rejection) power for electromagnetic showers. Electromagnetic and hadronic showers differ in their spatial development and energy distribution in a way that can be distinguished by the calorimeter. This is demonstrated in figure 14 which shows examples of an electromagnetic shower induced by an electron (left) and an interacting proton (right), recorded during tests with particle beams at the CERN SpS facility. All incident particles have a momentum of 50 GeV/c. The electron-hadron separation performance of the calorimeter has been extensively studied in [49] where it was shown that the rare antiproton and positron components in the cosmic radiation can be identified with a background at the percent level and lower, especially at scientifically interesting momenta  $>10$  GeV/c.

The calorimeter will also be used to reconstruct the energy of the electromagnetic showers. This will provide a measurement of the energy of the incident electrons independent from the magnetic spectrometer, thus allowing a cross-calibration of the two energy determinations. As shown in figure 15, the constant term for the calorimeter energy resolution has been measured as  $\sim 5.5\%$  for electromagnetic showers generated by particles entering the calorimeter within the acceptance of the tracking system up to an energy of several hundred GeV.

The calorimeter is also equipped with a self-trigger capability, as discussed in

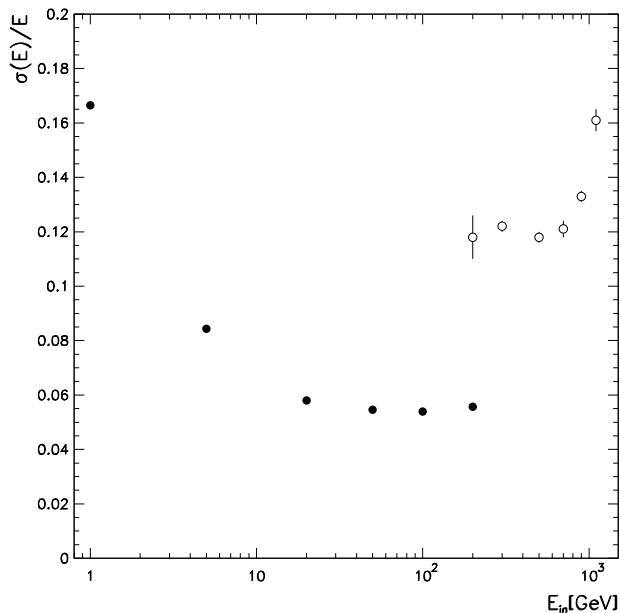


Fig. 15. The energy dependence of the energy resolution of the electromagnetic calorimeter. The filled symbols are for normal operation and the open symbols are for the self-trigger mode, described in section 3.

section 3.2.

### 2.6 Shower tail catcher scintillator

The shower tail catcher scintillator (S4) improves the PAMELA electron-hadron separation performance by measuring shower leakage from the calorimeter. It also provides a high-energy trigger for the neutron detector (described in the next section). This scintillator is placed directly beneath the calorimeter. It consists of a single square piece of 1 cm thick scintillator of dimensions  $(48 \times 48)$  cm<sup>2</sup> which is read out by six PMTs, as shown in figure 16.

### 2.7 Neutron detector

The neutron detector complements the electron-proton discrimination capabilities of the calorimeter. The evaporated neutron yield in a hadronic shower is 10–20 times larger than expected from an electromagnetic shower. The neutron detector is sensitive to evaporated neutrons which are thermalised in the calorimeter. The detection efficiency (including thermalisation) is  $\sim 10\%$ . Joint analysis of the calorimeter and neutron detector information will allow primary electron energies to be determined up to several TeV.



Fig. 16. Left: the shower tail catcher scintillator, S4, showing the 6 PMTs used for read-out. The scintillator has dimensions  $(48 \times 48)$  cm<sup>2</sup>. Right: The neutron detector partially equipped with <sup>3</sup>He proportional counters. The neutron detector covers an area of  $(60 \times 55)$  cm<sup>2</sup>.

The neutron detector [50] is located below the S4 scintillator and consists of 36 proportional counters, filled with <sup>3</sup>He and surrounded by a polyethylene moderator enveloped in a thin cadmium layer to prevent thermal neutrons entering the detector from the sides and from below. The counters are stacked in two planes of 18 counters, oriented along the y-axis of the instrument. The size of the neutron detector is  $(60 \times 55 \times 15)$  cm<sup>3</sup> and is shown in figure 16.

### 3 PAMELA data acquisition and trigger system

#### 3.1 Data acquisition system

A schematic overview of the PAMELA data acquisition (DAQ) system is shown in figure 17. The PSCU (PAMELA Storage and Control Unit) handles all slow controls, communication with the satellite, data acquisition, storage and downlink tasks. The PSCU contains 4 subsystems:

- (i) A processor module built around a CPU based on a ERC-32 architecture (SPARC v7 implementation) running the RTEMS real time operating system at 24 MHz. The CPU is custom built by Laben and is fully space qualified. Communication with the Resurs satellite is realised via a standard 1553B data-bus;
- (ii) Two redundant 2 GByte mass memory modules. The modules include latch-up detection, allowing operation to be transparently switched to the safe module when a latch-up is detected;
- (iii) A PIF (PAMELA interface board) that performs three main tasks: communication with the IDAQ (Intermediate DAQ) system through a DMA (dynamic memory access) controller, handling the interface with the mass

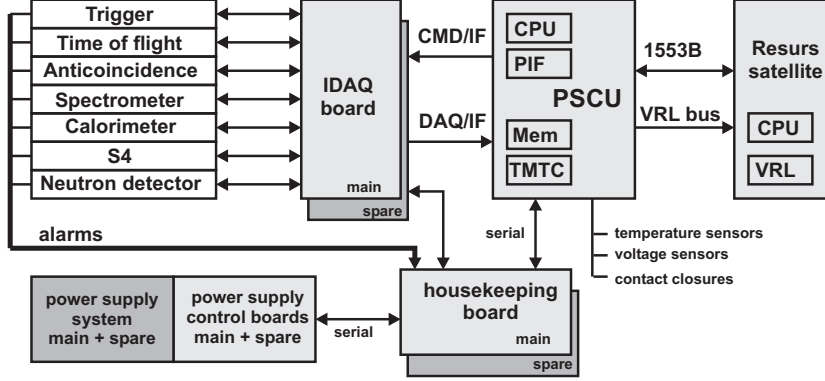


Fig. 17. Scheme of the PAMELA data acquisition system. The interfaces (IF) between the IDAQ and the PSCU handle the data acquisition and transfer the commands (CMD) to the IDAQ. The communication between PAMELA and the spacecraft is handled by the 1553B bus and by the link to the VRL module for data download to the Resurs memory. Adapted from [51].

- memory, and providing the interface with the VRL (Very high-speed Radio Link) module of the satellite;
- (iv) A TMTC (Telemetry and Control) board that handles the housekeeping operations of PAMELA, such as alarm, temperature and voltage monitoring (once per second). Such monitoring is performed both directly (ADC inputs and contact closure telemetries) and through a dedicated housekeeping board that communicates through serial data links with the subdetector read-out boards, with the IDAQ board and with the power supply control boards.

Data acquisition from the subdetectors is managed by the IDAQ system at a rate of 2 MByte/s. Upon receipt of a trigger, the PSCU initiates the IDAQ procedure to read out data from the subdetectors in sequence. The resulting data are stored in the PSCU mass memory. Several times a day, the data are transferred to the satellite on-board memory via the 12 MByte/s VRL bus where it is stored prior to downlinking to earth. Approximately 15 GBytes are transferred to ground per day during 2-3 downlink sessions.

The PSCU automatically handles the flow of PAMELA physics tasks and continuously checks for proper operation of the apparatus. At boot, the PSCU manages the operation of the power supply system to power up all subsystems, initializes all detectors and starts the data acquisition cycle. In parallel, once per second the PSCU checks the TMTC information on voltages and alarms. In case of abnormal conditions the PSCU can perform a hardware reset of the whole system or, if insufficient to solve the problem (e.g. in case of electronics latch-up), powers down and then up PAMELA. The PSCU also checks the temperature environment by reading dedicated temperature sensors distributed in various locations around the instrument. If the readings exceed predefined values (set with dedicated commands from ground) the PSCU

powers down PAMELA until acceptable working conditions are reached. The PSCU also handles communication with the Resurs satellite CPU and VRL system. Data is downloaded to the VRL upon receipt of a dedicated command from the Resurs CPU. The scheduling of data downloads from the PAMELA mass memory to the VRL hard disk system is defined from ground on a daily basis.

The PSCU organizes the data acquisition cycle in “runs”. A run is defined as a continuous period of data taking in which the trigger and detector configurations are constant. These configurations are defined by the PSCU according to information stored in on-board memory or received from ground. The duration of a run is determined by the PSCU according to the orbital position (e.g. inside radiation belts or South Atlantic Anomaly SAA or outside these areas). The orbital position also dictates the trigger configuration, as described in the following section. The orbital position is derived from the “ascending node” notification issued by the Resurs CPU when the satellite crosses the equator from the southern hemisphere to the northern hemisphere. From this position information, the CPU extrapolates the entry time into high radiation environments. This can be performed in three ways, chosen from ground:

- when the counting rate of the S1 scintillator exceeds a given threshold (changeable from ground with dedicated command);
- according to fixed time periods conservatively chosen and modifiable from ground;
- according to a table with crossing times in absolute Moscow time<sup>2</sup> provided on a bi-weekly basis from ground with a dedicated command.

Additionally, the PSCU can interrupt and close a run if anomalous conditions that require action upon the subsystems (e.g. hardware resets, etc.) are detected.

Periodically the PSCU calibrates the detectors, namely the anticounter system, the tracker, the calorimeter and the S4 scintillator. By default, the calibration is performed at the point of lowest cosmic-ray trigger rate, i.e. the equator, upon receiving an “ascending node” notification from the Resurs CPU. The frequency of calibrations can be modified from ground.

### 3.2 *Trigger system*

The PAMELA trigger condition is defined by coincident energy deposits in the scintillator ToF layers. Various configurations can be selected. The default

---

<sup>2</sup> On a regular basis the Resurs CPU sends a time synchronization command with the Moscow time to the PSCU. The precision of this information is  $\sim 1$  s.

ones (the subscripts 1 and 2 refer to the upper and lower layers in each ToF plane) used outside and inside radiation environments are:

- ( $S_{1_1}$  or  $S_{1_2}$ ) and ( $S_{2_1}$  or  $S_{2_2}$ ) and ( $S_{3_1}$  or  $S_{3_2}$ ) outside radiation belts and SAA;
- ( $S_{2_1}$  or  $S_{2_2}$ ) and ( $S_{3_1}$  or  $S_{3_2}$ ) inside radiation belts and SAA;

since, according to simulation, the radiation environment will saturate the S1 counting rate but will not affect significantly the S2 and S3 scintillators since they are more shielded.

These trigger configurations can be changed from ground with dedicated commands to the PSCU. A total of 29 configurations have been implemented on the trigger board. Various combination of *and* or *or* of the scintillators layers with or without the calorimeter self-trigger and S4 trigger (described below) are implemented. The PMTs can be masked on the trigger board by the PSCU.

The calorimeter is equipped with a self-trigger capability. A trigger signal is generated when a specific energy distribution is detected in predetermined planes within the lower half of the calorimeter. The sets of planes used in this configuration can be changed with a dedicated command from ground. This allows PAMELA to measure very high-energy ( $\sim 300$  GeV to  $>1$  TeV) electrons in the cosmic radiation. At present, very few measurements have covered this energy range [52]. Since these events are rare, it is important to have a large geometrical factor. By requiring that triggering particles enter through one of the first four planes and cross at least 10 radiation lengths, the geometrical factor is  $\sim 600$  cm<sup>2</sup>sr, i.e. about a factor of 30 larger than the default PAMELA acceptance defined by the magnetic spectrometer. The behavior of the calorimeter in self-trigger mode has been studied by means of simulations [53]. The simulated energy resolution of the calorimeter in self-trigger mode is approximately constant ( $\sim 12\%$ ) up to about 800 GeV, as shown in figure 15. At higher energies the resolution decreases because of increasing longitudinal leakage and saturation of the signal from the strips (about 1000 mip). The choice of energy loss and activated planes implemented in the calorimeter electronics to generate a trigger signal has been taken to have the highest proton rejection while keeping a trigger efficiency of better than 90% for electrons of energies higher than 300 GeV [53]. Combined with the neutron detector information, the apparatus will be able to cleanly identify very high-energy electrons. The neutron detector can also be triggered when an energy deposit exceeding 10 mip is detected in the S4 scintillator.

The trigger rate observed during a typical orbit is shown in figure 18. The maxima at  $\sim 2000$  events per minute ( $\sim 30$  Hz) correspond to passages over the polar regions (North Pole, NP and South Pole, SP) while the minima ( $\sim 15$  Hz) correspond to equatorial regions (E). The contribution from the South Atlantic



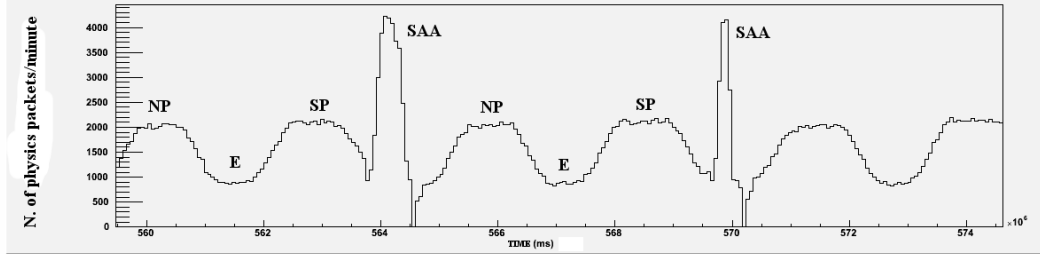


Fig. 18. The PAMELA trigger rate shown in events per minute evaluated during an arbitrary orbit (period  $\sim 94$  minutes). The trigger rate is strongly dependent on the orbital position : NP, North Pole; SP, South Pole; E, Equator; SAA , South Atlantic Anomaly (SAA).

Anomaly (SAA) is clearly visible ( $\sim 70$  Hz). Note that data is taken in the SAA using the second default trigger configuration. The missing acquisition time after the peaks of the SAA corresponds to the detector calibrations upon crossing the equator (about 1 minute in duration).

If the amount of event data exceeds the storage dedicated to PAMELA on-board the Resurs satellite or the daily downlink limit, an on-line event selection is provided by a second level trigger. The second level trigger is not normally activated and must be activated via an uplinked command from ground. Information from the CAS anticoincidence system is used to reject “false” triggers (see section 2.3) and information from the calorimeter are used to reduce the impact of particles backscattered from the calorimeter. The second level trigger is described in detail elsewhere [44].

#### 4 The Resurs DK1 satellite

The Resurs DK1 satellite is manufactured by the Russian space company TsSKB Progress to perform multi-spectral remote sensing of the Earths surface and acquire high-quality images in near real-time. Data delivery to ground is realised via a high-speed radio link.

The satellite is presented in figure 19, has a mass of  $\sim 6.7$  Tonnes and a height of 7.4 m. The solar array span is  $\sim 14$  m. The satellite is three-axis stabilized with an axis orientation accuracy of 0.2 arcmin and an angular velocity stabilization accuracy of  $0.005^\circ/\text{s}$ . The orbital altitude varies between 350 km and 600 km at an inclination of  $70^\circ$ . The design lifetime is three years.

PAMELA is mounted in a dedicated Pressurized Container (PC) attached to the Resurs DK1 satellite. During launch and orbital manoeuvres, the PC is secured against the body of the satellite. During data-taking it is swung up to give PAMELA a clear view into space. The container is cylindrical in shape

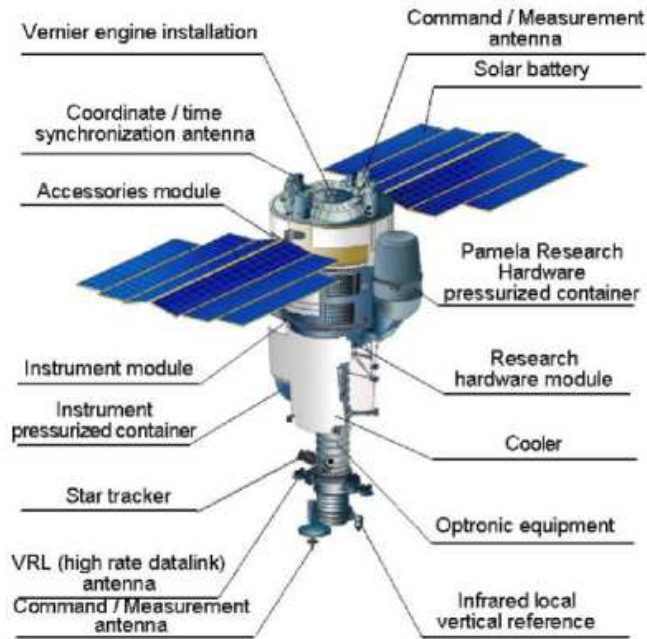


Fig. 19. A sketch of the Resurs DK1 satellite which hosts the PAMELA experiment in a Pressurized Container (shown in the data-taking position). The satellite has a height of 7.4 m.



Fig. 20. Tests of the PAMELA Pressurized Container during orbital operations (May 2002). The body of the Resurs DK1 satellite can be seen to the right of the picture.

and has an inside diameter of about 105 cm, a semi-spherical bottom and a conical top. It is made of an aluminum alloy, with a thickness of 2 mm in the acceptance of PAMELA. Figure 20 shows tests of the PC tilting mechanism performed in May 2002 at the TsSKB Progress facility in Samara. The movement of the PC from the parked to the data-taking position was tested in simulated weightless conditions.

#### 4.1 *NTs OMZ ground segment*

The ground segment of the Resurs DK1 system is located at the Research Center for Earth Operative Monitoring (NTs OMZ) in Moscow, Russia [54]. This forms part of the Russian Space Agency (Roskosmos) ground segment designed for acquiring, recording, processing and distributing data from remote sensing systems in space.

The reception antenna at NTs OMZ is a parabolic reflector of 7 m diameter, equipped with an azimuth-elevation rotation mechanism, and has two frequency multiplexed radio channels. The Resurs DK1 radio link towards NTs OMZ is active 2-3 times a day. The average volume of data transmitted during a single downlink is currently  $\sim 6$  GBytes, giving a total of 15 GBytes/day. Data received from PAMELA are collected by a data-set archive server. The server calculates the downlink session quality (the error probability per bit) and faulty downlink sessions can be assigned for retransmission up to several days after the initial downlink. The downlinked data are transmitted to a server dedicated to data processing for instrument monitoring and control, and is also written to magnetic tape for long-term storage. All such operations are automatized to minimize the time delay between the data reception and the extraction of monitoring information.

After this first level of data analysis, both raw and preliminary processed data are moved through a normal internet line to the main storage centre in Eastern Europe, which is located at MePHI (Moscow, Russia). From here, GRID infrastructure is used to move raw and first level processed data to the main storage and analysis centre of the PAMELA Collaboration, located at CNAF (Bologna, Italy), a specialized computing centre of INFN. Here data are accessible to all various institutions within the PAMELA collaboration.

## 5 **Qualification tests**

Space-borne apparatus must maintain a high level of performance and stability throughout the mission duration in the harsh environment of space. The mechanical design must be such that the payload and satellite withstand the significant shocks and vibrations of the launch. The extremes of temperature that may be encountered in space requires that the thermal and mechanical designs be such that the sensitive components maintain excellent stability over a broad range of temperatures. The radiation environment in space is major consideration in the design of electronic circuitry. All chosen components must be tested for radiation tolerance prior to use. Electromagnetic interference (EMI) from electronic devices must be minimized by the use of different

types of filters and shielded cables.

In this section the steps taken to qualify PAMELA for operation in space are reviewed.

### *5.1 Radiation tolerance*

In orbit all on-board electronic devices will be subject to the passage of ionizing particles, which can degrade their performance and eventually lead to their permanent damage or loss of functionality. Since malfunctioning components cannot be replaced once the instrument is in orbit, all critical devices must either be already space qualified, or tested for radiation tolerance before use.

For economic, performance and power consumption reasons, most of the PAMELA electronic components are “off-the-shelf” commercial products. Radiation tolerance tests therefore had to be carried out before their integration into electronic boards. A selection of electronic components have been tested under gamma and heavy ion beams during the construction phase of the PAMELA subsystems.

As an example, the DSP and FPGA chips used through-out the PAMELA data acquisition system were extensively tested in the period 2000-2002, using heavy-ion beams. The tests were performed at GSI in Darmstadt (Germany), and JINR in Dubna (Russia). At GSI the devices were exposed to beams of  $^{131}\text{Xe}$  and  $^{238}\text{U}$ , in the energy range 100-800 MeV/n. Different incidence angles allowed different doses to be achieved. At JINR slow beams of  $^{24}\text{Mg}$  at 150 MeV/n were used, in order to maximize the energy transfer to the components under test. Test results have been published elsewhere [55].

### *5.2 Mechanical Qualification*

The mechanical and thermal space qualification tests of the PAMELA instrument were performed in the years 2002-2003. In order to perform such tests, a mock-up of the entire instrument, Mass-Dimensional and Thermal Model (MDTM), was manufactured. The MDTM reproduces the geometrical characteristics of PAMELA (e.g. dimensions, total mass, center of gravity, inertial moments) and the basic thermal behavior. All particle detectors in the MDTM were simulated by dummy aluminum boxes. The electronics systems were non-functional and only reproduced the power consumption of each subsystem.

In order to ensure that no damage occurs to PAMELA or the spacecraft during any of the different operational phases of the mission (transport, launch,



Fig. 21. The PAMELA MDTM on the shaker system in IABG (August 2002).

orbital operations, unlocking of the Pressurized Container, flight), the MDTM was exposed to vibration spectra at mechanical loads exceeding those expected during the mission. The MDTM vibration tests were performed at IABG Laboratories (Munich, Germany) in August 2002, as shown in figure 21. During the test it was verified that structural integrity was maintained and that there was no change in the dynamic behavior of MDTM (using resonance searches). The MDTM structure was subjected to the required vibration loads along three orthogonal axes. Additional transport, vibration and shock tests of the MDTM whilst integrated into the Pressurized Container were performed at the TsSKB-Progress Testing Center in May 2003. Additional information about PAMELA mechanical space qualification can be found in [56].

### 5.3 Thermal Qualification

The PAMELA thermal cooling system consists of a 8.6 m long pipe that joins 4 radiators and 8 flanges connected throughout the PAMELA detector system. The task of this system is to dissipate the heat produced by the PAMELA subsystems and transfer it into the spacecraft, where a custom designed thermal control system is located. This transfer is performed by means of a heat-transfer fluid pumped by Resurs satellite through the PAMELA pipelines. The total heat release of PAMELA cannot exceed 360 W.

Thermal and vacuum tests of the PAMELA MDTM were performed in the laboratories of TsSKB-Progress in April 2003. Six thermal modes of operation were implemented, where the three relevant parameters which regulate the instrument thermal behaviour (PAMELA power consumption, external heat flows and heat-transfer fluid temperature and flow rate) were varied between

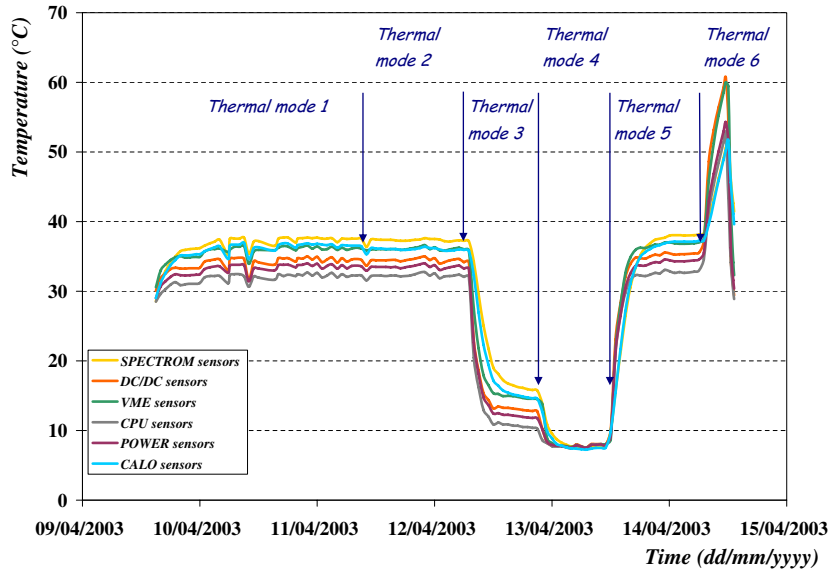


Fig. 22. Results of the PAMELA thermal qualification tests. Temperatures in different subsystems are shown during the execution of the 6 different thermal modes. The temperature remained always between acceptable limits ( $5^{\circ}\text{C}$  -  $40^{\circ}\text{C}$ ) except for thermal mode number 6 where a stop in the heat transfer fluid was simulated.

the design extrema to simulate in-flight operations. Each mode persisted until a steady state condition was reached. As an example, a test simulating an interruption in the flow of the heat-transfer fluid due to a malfunctioning was interrupted after 3 hours when the PAMELA MDTM reached a temperature of  $\sim 60^{\circ}\text{C}$ .

The qualification test of the PAMELA thermal system showed that all parameters of the system stayed within the design limits ( $5^{\circ}\text{C}$  -  $40^{\circ}\text{C}$ ). During the Resurs DK1 orbit, the operating temperature range of PAMELA will vary between  $7^{\circ}\text{C}$  for the coldest systems and  $38^{\circ}\text{C}$  for the warmest ones, as shown in figure 22.

Additional information about PAMELA thermal space qualification can be found in [56].

#### 5.4 Electrical tests

To perform tests of the electrical interface between PAMELA and the spacecraft, a second mock-up of the PAMELA instrument was assembled. This “Technological Model” was an exact copy of the Flight Model from the point of view of electrical connections to the satellite and for the readout electronics boards, with the particle detectors substituted by dummies. The Technological Model was shipped to TsSKB-Progress in April 2004 (see figure 23). The



Fig. 23. The PAMELA Technological Model during transportation from Rome to the TsSKB-Progress plant (April 2004).

task of the Technological Model was to thoroughly test the electrical interface to the Resurs DK1 satellite. In addition, it was used to check that the residual magnetic field from the PAMELA spectrometer did not interfere with the Resurs instrumentation. These complex tests proceeded in phases. A first test was performed in Rome in December 2003, with the satellite emulated by a Ground Support Equipment (EGSE) system. A second test started in May 2004 at TsSKB-Progress and verified the powering procedures. In October 2004 the PAMELA Technological Model was fully integrated into the Resurs DK1 to complete all remaining tests.

## 6 Physics Performance

### 6.1 Beam tests

Between July 2000 and September 2003, the PAMELA subsystems were periodically exposed to particle beams at the CERN PS and SPS facilities. Electron and proton beams were used with energies in the 10's - 100's GeV range. Results from these tests are described in section 2.

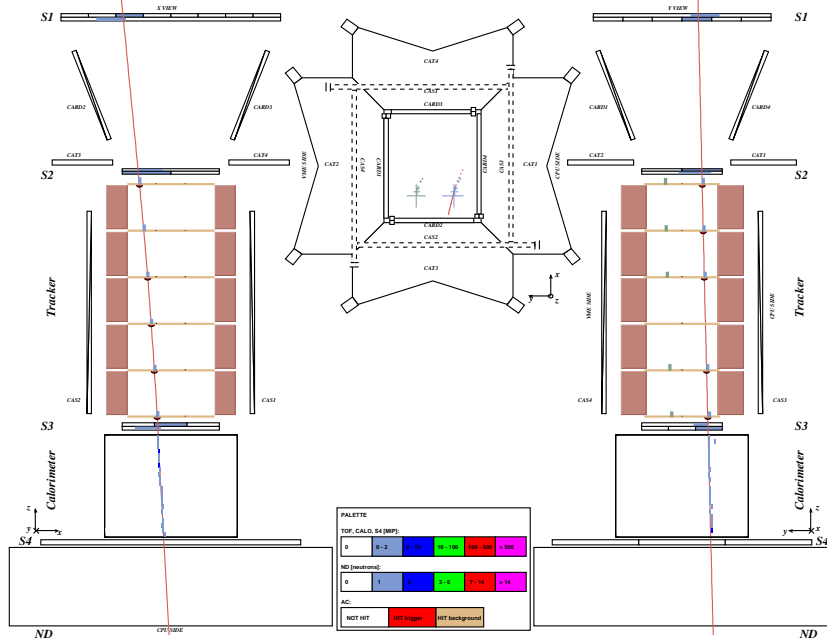


Fig. 24. The event display of a  $1.5 \text{ GeV}/c \mu^-$  from ground data. On the left (right) the x, bending view (y-view) of PAMELA are indicated. A plan view of PAMELA is shown in the centre. The signals as detected by PAMELA detectors are shown along with the particle direction (solid lines) reconstructed by the fitting procedure of the tracking system.

## 6.2 Ground data

Prior to delivery to Russia, the PAMELA instrument was assembled at the INFN laboratories of Roma Tor Vergata, Rome, Italy. The system was tested with cosmic rays over a period of several months. Figures 24 and 25 show two cosmic ray events recorded in Rome. The first is a  $1.5 \text{ GeV}/c$  negatively charged particle, with high probability of being a  $\mu^-$  considering the clean non-interacting pattern in the calorimeter. The second is a  $67 \text{ GeV}/c$  particle with an hadronic interaction in the calorimeter, consistent with a proton. All PAMELA detectors are shown in the figures along with the signals produced by the particles in the detectors and derived information. Highly detailed information is provided for each cosmic-ray event. The solid lines indicate the tracks reconstructed by the fitting procedure [57] of the magnetic spectrometer. The figures show also the “ghost” hits due to the common readout of the 2 silicon sensors of the same ladder in the non-bending projection. This ambiguity is solved with the help of track fitting procedure and with a consistency check with the other Pamela subdetectors.

The muon charge ratio measured at ground in Rome (50 m above sea level) has been obtained and is presented in figure 26. Muons were selected as non-interacting particles in the calorimeter and having unit charge in the ToF



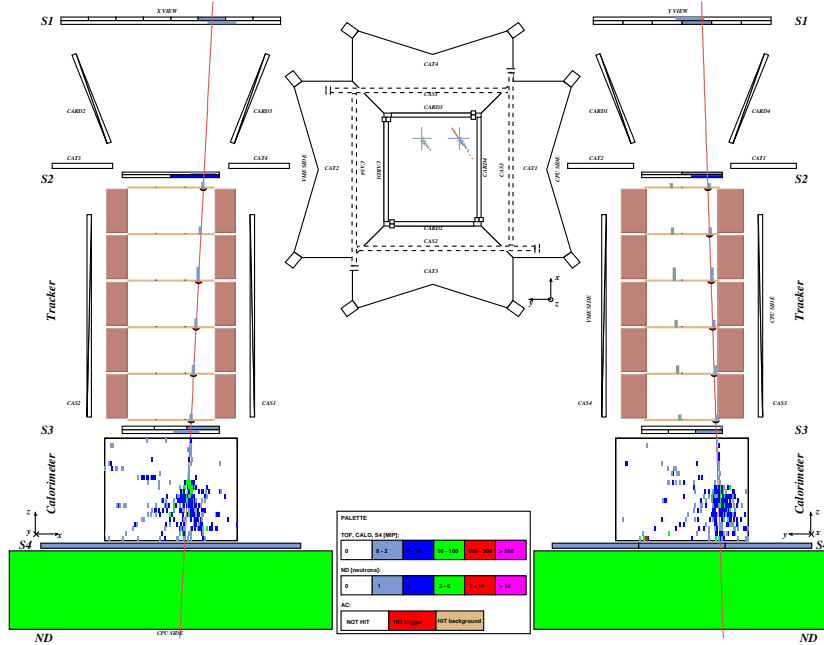


Fig. 25. The event display of a 67 GeV/c hadron from ground data. On the left (right) the x, bending (y-view) of PAMELA are indicated. A plan view of PAMELA is shown in the centre. The signals as detected by PAMELA detectors are shown along with the particle direction (solid lines) reconstructed by the fitting procedure of the tracking system.

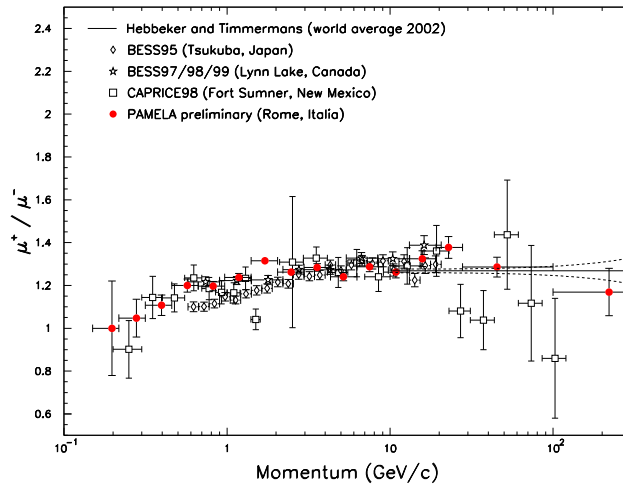


Fig. 26. The muon charge ratio measured at ground by PAMELA compared with the 2002 global fit of experimental data by Hebbeker and Timmermans [58] and more recent experimental results [59,60]. The dashed lines indicate a one standard deviation of the fit.

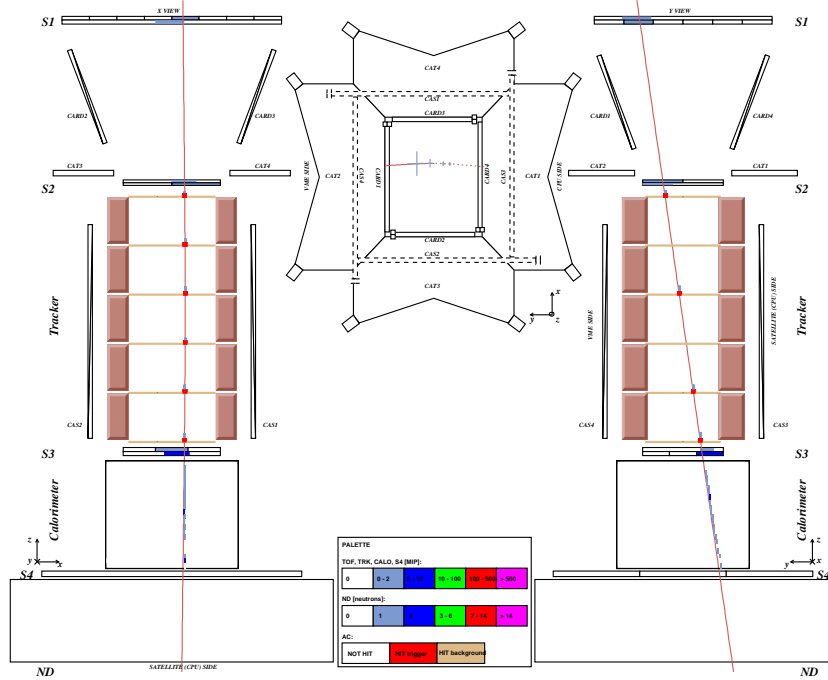


Fig. 27. The event display of a  $\sim 3$  GV non-interacting proton from flight data. On the left (right) the x, bending view (y-view) of PAMELA are indicated. A plan view of PAMELA is shown in the centre.

scintillators. Additionally, low-energy protons were rejected based on the ionization losses in the calorimeter. Momenta were determined by the magnetic spectrometer. The PAMELA data agree well with other published results [58,59,60].

### 6.3 In-orbit performance

PAMELA was successfully launched on June 15<sup>th</sup> 2006 and was first switched-on on the 20<sup>th</sup> of June. After a brief period of commissioning PAMELA has been in a continuous data-taking mode since July 11<sup>th</sup>. Data downlinked to ground show that the entire instrument is working as expected. Figure 27 shows a 3 GV non-interacting proton recorded in-orbit while figure 28 shows a 13 GV helium nucleus interacting in the calorimeter. The in-orbit performance of PAMELA will be discussed in future publications.

## 7 Conclusions

PAMELA is a multi-purpose satellite-borne apparatus designed to study charged particles in the cosmic radiation with a particular focus on antiparticles (an-

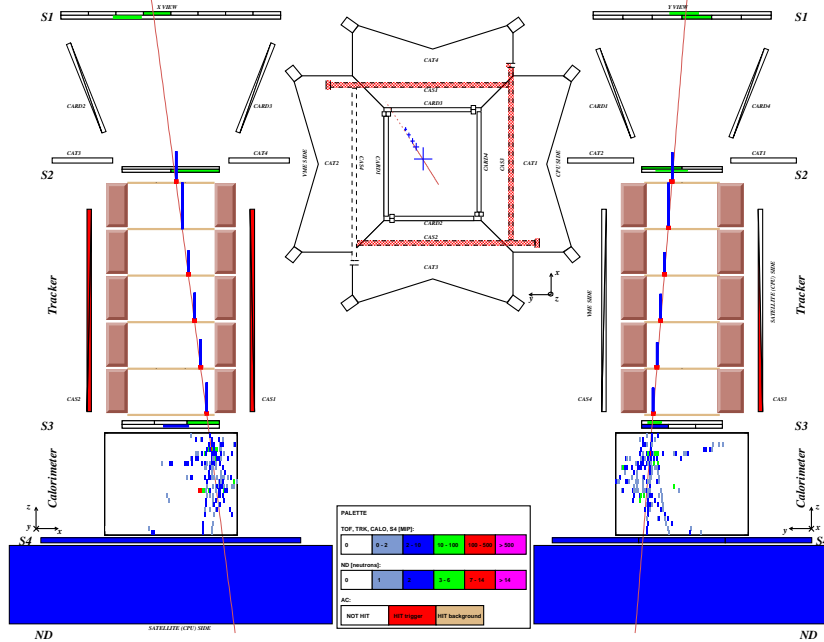


Fig. 28. The event display of a  $\sim 13$  GV interacting helium nucleus from flight data. On the left (right) the x, bending (y-view) of PAMELA are indicated. A plan view of PAMELA is shown in the centre. Note the increased energy deposit in the silicon tracker planes (denoted by the vertical bars) compared to figure 27. The activity in the anticounter system is probably due to secondary particles backscattered from the calorimeter.

tiprotons and positrons). The energy range over which observations are made and the foreseen statistics means that PAMELA stands to deliver results of great scientific relevance in several fields of cosmic ray research. To ensure reliable operation in space extensive space qualification tests of the PAMELA detector systems, electronics and mechanical structures was performed prior to launch. The performance of the individual detector components and the PAMELA system as a whole were also verified at particle beam facilities. The PAMELA instrument was launched into orbit from the Baikonur Cosmodrome on-board a Resurs DK1 satellite on June 15<sup>th</sup> 2006. All systems have been observed to operate as expected and scientific data analysis is now on-going.

## 8 Acknowledgments

The PAMELA mission is sponsored by the Italian National Institute of Nuclear Physics (INFN), the Italian Space Agency (ASI), the Russian Space Agency (Roskosmos), the Russian Academy of Science, the German Space Agency (DLR), the Swedish National Space Board (SNSB) and the Swedish Research Council (VR). PAMELA is the result of a collaborative work that has lasted for several years. We gratefully acknowledge the contributions from

the Italian companies Carlo Gavazzi Space, Laben, CAEN, Kayser, Forestal and Aerostudi. We also would like to thank the scientific laboratories and test facilities that assisted the PAMELA team during the qualification phases : CERN (Geneva, Switzerland), JINR (DUBNA, Russia), GSI (Darmstadt, Germany), IABG (Munich, Germany), ENEA-CASACCIA (Rome, Italy) and GALILEO (Florence, Italy). We also thank the following engineers and technicians for their valuable contribution to the project : L. Andreanelli, E. Barbarito, A. Bazarov, F. Ceglie, S. Ciano, C. Fiorello, M. Franco, A. Gabbanini, E. Gaspari, M. Grandi, M. Lundin, G. Mazzenga, M. Mongelli, R. Möllerberg, O. Panova, P. Parascandolo, G. Passeggio, G. Pontoriere, E. Reali, R. Rocco, S. Rydström, A. Sedov, B. Talalaev, M. Tesi, E. Vanzanella, and V. Zotov. We thank the data reception centre, NTs OMZ, for its first class preparation of the PAMELA data receiving station in Moscow. Finally, we would like to express our gratitude to TsSKB-Progress, who carefully followed the PAMELA mission during all its phases and made the PAMELA launch a reality.

## References

- [1] Y. Asaoka et al., Phys. Rev. Lett. 88 (2002) 051101; astro-ph/0109007 (2001).
- [2] K. Maki et al., Phys. Rev. Lett. 76 (1996) 3474.
- [3] L. Bergström et al., Phys. Rev. D 59 (1999) 43506.
- [4] D. Hooper et al., Phys.Rev. D 71 (2005) 083503.
- [5] T. Bringmann, JCAP 08 (2005) 006; astro-ph/0506219 (2005).
- [6] M. Simon et al., Astrophys. J. 499 (1998) 250.
- [7] L. Bergström and P. Ullio, private communication (1999).
- [8] R.J. Protheroe, Astrophys. J. 254 (1982) 391.
- [9] I.V. Moskalenko et al., Astrophys. J. 493 (1998) 694.
- [10] P. Ullio, astro-ph/9904086 (1999).
- [11] E.A. Baltz et al., Phys. Rev. D 59 (1999) 023511.
- [12] H. Aizu et al., Phys. Rev. 121 (1961) 1206; P. Evenson, Astrophys. J. 176 (1972) 797; G.F. Smoot et al., Phys. Rev. Lett. 35 (1975) 258; G.D. Badhwar et al., Nature 274 (1978) 137; A. Buffington et al., Astrophys. J. 248 (1981) 1179; R.L. Golden et al., Astrophys. J. 479 (1997) 992; J.F. Ormes et al., Astrophys. J. Lett. 482 (1997) L187; T. Saeki et al., Phys. Lett. B 422 (1998) 319; J. Alcaraz et al., Phys. Lett. B 461 (1999) 387; M. Sasaki et al., Nucl. Phys. (Proc. Suppl.) B 113 (2002) 202.
- [13] P. Everson, Astrophys. J. 176 (1972) 797.

- [14] J. Lund, “Antiparticle Identification Studies for the PAMELA Satellite Experiment”, PhD thesis, KTH, Stockholm (2004).
- [15] M. Casolino et al., *Advances in Space Research* 37 (2006) 1848.
- [16] A.M. Atoyan et al., *Phys. Rev. D* 52 (1995) 3265.
- [17] M. Aguilar et al., *Phys. Rep.* 366 (2002) 331.
- [18] M. Boezio et al., *Astrophys. J.* 561 (2001) 787; astro-ph/0103513 (2001).
- [19] S. Orito et al., *Phys. Rev. Lett.* 84 (2000) 1078.
- [20] G. Basini et al., *Proc. 26th International Cosmic Ray Conference, Salt Lake City, Vol 3* (1999) 77; M. Hof et al., *Astrophys. J.* 467 (1996) L33.
- [21] M. Boezio et al., *Astrophys. J.* 487 (1997) 415.
- [22] J. Mitchell et al., *Phys. Rev. Lett.* 76 (1996) 3057.
- [23] R.L. Golden et al., *Astron. & Astrophys.* 188 (1987) 145.
- [24] D. Müller et al., *Astrophys. J.* 312 (1987) 183.
- [25] J.M. Clem et al., *Astrophys. J.* 464 (1996) 507.
- [26] R.L. Golden et al., *Astrophys. J.* 436 (1994) 769.
- [27] R.L. Golden et al., *Astrophys. J.* 457 (1994) L103.
- [28] S.W. Barwick et al., *Astrophys. J.* 498 (1998) 779.
- [29] M. Boezio et al., *Astrophys. J.* 532 (2000) 653; G. Barbiellini et al., *Astron. & Astrophys.* 309 (1996) L15.
- [30] J. Alcaraz et al., *Phys. Lett. B* 484 (2000) 10.
- [31] M. Boezio et al., *Advances in Space Research* 27 (2001) 669.
- [32] J.J. Beatty et al., *Phys. Rev. Lett.* 93 (2004) 241102; astro-ph/0412230 (2004).
- [33] <http://www.actel.com>
- [34] <http://www.analog.com>
- [35] S.B. Ricciarini, “Development of tracking system acquisition electronics and analysis of first data for the PAMELA experiment”, PhD Thesis, University of Florence (2005).
- [36] G. Osteria et al., *Nucl. Instr. and Meth.* A535 (2004) 152.
- [37] <http://www.bicron.com>
- [38] G. Osteria et al., *Nucl. Instr. and Meth.* A518 (2004) 161.
- [39] J. Lund, “A Study of the PAMELA Anticoincidence System”, licentiate thesis, KTH, Stockholm (2002).

- [40] S. Orsi et al., Proc. 29th International Cosmic Ray Conference, Pune, Vol. 3 (2005) 369.
- [41] S. Orsi et al., Advances in Space Research 37 (2006) 1853.
- [42] <http://www.tyvek.com>
- [43] J. Lundquist, "The Anticoincidence System of the PAMELA Satellite Experiment". PhD thesis, KTH, Stockholm (2006).
- [44] S. Orsi et al., Astroparticle Physics 25 (2006) 33.
- [45] M. Pearce et al., Nucl. Instr. and Meth. A488 (2002) 536.
- [46] O. Adriani et al., Nucl. Instr. and Meth. A 511 (2003) 72.
- [47] <http://www.ideas.no>
- [48] V. Bonvicini, "The CR1.4P: an integrated front-end circuit for the Imaging Calorimeter of PAMELA", 5th International Workshop on Front-end Electronics "FEE 2003", Snowmass (2003).
- [49] M. Boezio et al., "The electron-hadron separation performance of the PAMELA electromagnetic calorimeter", Astroparticle Physics. Accepted for publication (2006).
- [50] Y. Stozhkov et al., Proc. 19th European Cosmic Ray Symposium, Florence (2004). International Journal of Modern Physics A 20 (2004) 6745.
- [51] M. Casolino et al., Advances in Space Research 37 (2006) 1857.
- [52] T. Kobayashi et al., Proc. 26th International Cosmic Ray Conference, Salt Lake City, Vol. 3 (1999) 61.
- [53] M. Boezio et al., Nucl. Instr. and Meth. A 487 (2002) 407; physics/0109010 (2001).
- [54] <http://eng.ntsomz.ru>
- [55] M. Boscherini et al., Nucl. Instr. and Meth. A 514 (2003) 112.
- [56] R. Sparvoli et al., Advances in Space Research 37, 1841 (2006).
- [57] O. Adriani et al., Proc. 29th International Cosmic Ray Conference, Pune, Vol. 3 (2005) 317.
- [58] T. Hebbeker et al., Astroparticle Physics 18 (2002) 107.
- [59] M. Motoki et al., Astroparticle Physics 19 (2003) 113.
- [60] M. Boezio et al., Phys. Rev. D 67 (2003) 072003.